Supporting Information

Acid-triggered two-stage superlarge redshift absorption for turn-on type photothermal conversion at first and second near-infrared window

Xiao-Qi Xu,[a] Yingchao Ma,[a] Ning-jiu Zhao,[b] Shangjie Tian,[c] Hechang Lei [c] and Yapei Wang*[a]

a. Key Laboratory of Advanced Light Conversion Materials and Biophotonics, Department of Chemistry, Renmin University of China, Beijing 100872.

b. State Key Laboratory of Molecular Reaction Dynamics, Dalian Institute of Chemical Physics, Chinese Academy of Sciences (CAS), Dalian 116023, China.

c. Department of Physics and Beijing Key Laboratory of Opto-electronic Functional Materials & Micro-nano Devices, Renmin University of China, Beijing 100872, China.

Materials

All commercially available chemicals were used without further purification unless otherwise noted. Aniline and 4-aminodiphenylamine was purchased from Shanghai Energy Chemicals Co., Ltd. p-phenylenediamine was purchased from Meryer (Shanghai) Chemical Technology Co., Ltd. 1,4-dibromobenzene, sodium tert-butoxide (NaO(*t*-Bu)), bis(dibenzylideneacetone) palladium ($Pd(dba)_2$), 1.1'-Binaphthyl-2.2'-diphemyl phosphine (rac-BINAP), and trifluoroacetic acid (TFA) were purchased from Meryer (Shanghai) Chemical Technology Co., Ltd. Triethylamine (TEA) was purchased from Shanghai Aladdin Bio-chem Technology Co., Ltd. Ferric chloride hexahydrate ($FeCl_3 \cdot 6H_2O$), ammonium peroxydisulfate ($(NH_4)_2S_2O_8$), ammonia solution ($NH_3 \cdot H_2O$), and 36% hydrochloric acid (HCl) solution supplied by Beijing Chemical Works. All organic solvents, including dimethyl sulfone (DMSO), ethanol (EtOH), dimethylformamide (DMF), and acetone were purchased from Beijing Tongguang Fine Chemicals Company.

Instruments

^1H NMR and ^{13}C NMR spectra were recorded on a Bruker 400 MHz spectrometer.

Ultraviolet-visible-near-infrared (UV-vis-NIR) absorption spectra of all the oligoaniline solutions were recorded by a SHIMADZU UV3600 spectrometer. High-resolution mass spectra (HRMS) were acquired on Thermo Q-Exactive instrument (quadrupole mass analyzer) using electrospray ionization mode (ESI). Electron paramagnetic resonance spectra were measured by JEOL JES-FA200 Electron Spin Resonance Spectrometry. Superconducting quantum interference device (SQUID) magnetometry was characterized by Quantum Design magnetic property measurement system (MPMS-3).

Experiment section

Synthesis and characterizations

Aniline trimer (3AT)

3AT was synthesized according to previous reports. In general, 1.86 g of aniline (Mw=93.13 g/mol) and 1.08 g of p-phenylenediamine (Mw=108.14 g/mol) were dissolved in a mixed solvent including 100 mL of 1 M HCl and 40 mL of EtOH. After the mixture was cooled down to -5 ^{o}C in an ice-salt bath, the solution of 4.5 g $(NH_4)_2S_2O_8$ (Mw=228.19 g/mol) in 1.0 M HCl was added dropwise for 30 min. The mixtures were stirred vigorously for another 4 h and filtered to obtain a precipitated product. Then, the filtered residue was added into 1.0 M $NH_3{\cdot}H_2O$ solution for deprotonation. After stirring for 1 h, the obtained mixture was filtered again and washed with 1.0 M $NH_3{\cdot}H_2O$ solution and distilled water. The blue solid product of 3AT was finally dried under vacuum at 45 ^{o}C for 48 h. The yield of 3AT was 58%. ^{1}H NMR (DMSO-*d6*, 400 MHz, ppm): δ 6.96 (*s*, 4H), 6.80-6.77 (*d*, 4H), 6.62-6.60 (*d*, 4H), 5.46 (*s*, 4H). ^{13}C NMR (DMSO-*d6*, 100 MHz, ppm): 142.60, 138.50, 134.87, 120.13, 117.49, 115.42. MS (ESI) calculated for C18H16N4 [M]: 288.1375. Found: 289.1445 $[M+H]^{+}$.

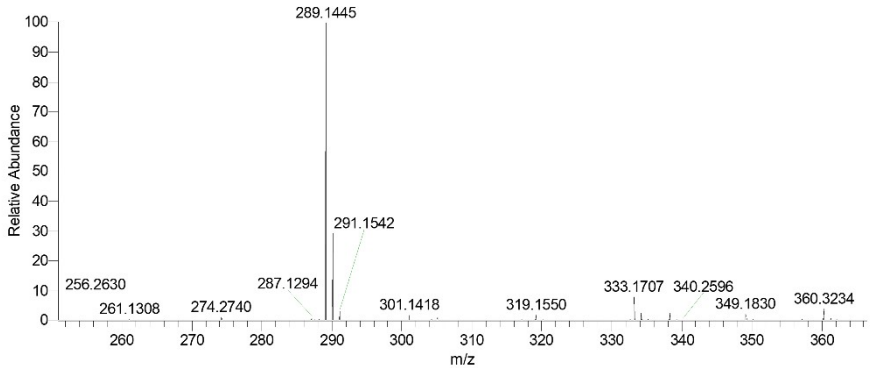

Figure S1. MS (ESI) spectrum of 3AT.

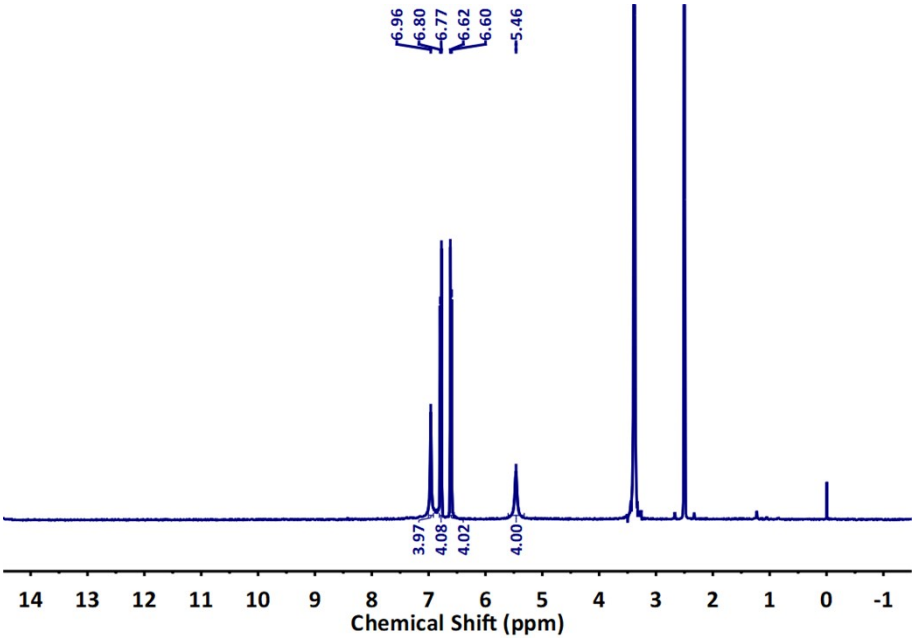

Figure S2. ^{1}H NMR spectrum of 3AT.

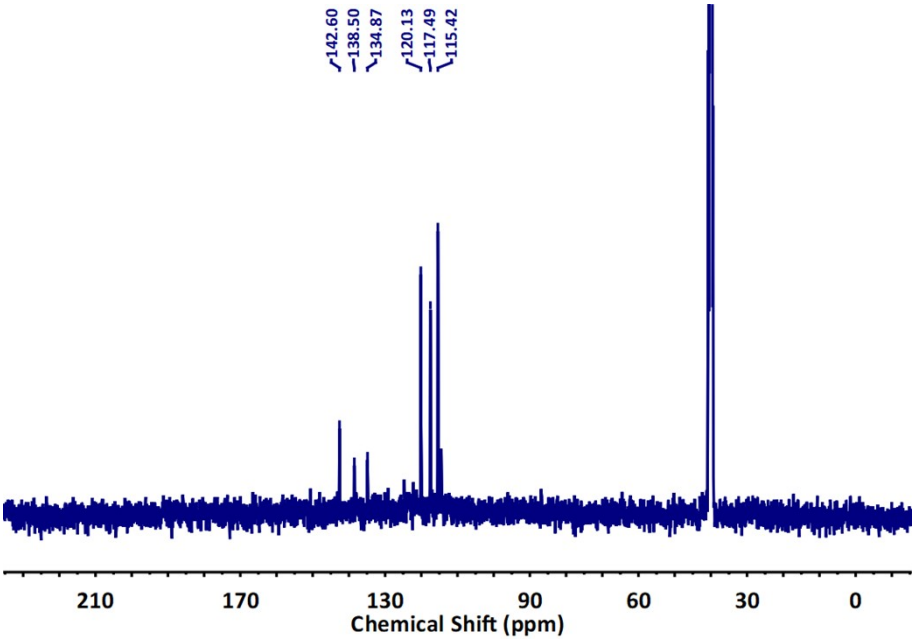

Figure S3. ^{13}C NMR spectrum of 3AT.

Aniline tetramer (4AT)

The synthesis of 4AT was carried out according to previous researches. Typically, 9.20 g of 4-aminodiphenylamine (Mw=184.24 g/mol) and was added into a round bottomed flask charged with 350 mL of diethyl ether. The mixture was then added with 75 mL of 2.0 M HCl solution.

After vigorous stirring for 4 h, the precipitated dianiline was collected via filtration and dried under vacuum for 24 h. The obtained dianiline (2.56 g, 10 mmol) was added into a 250 mL round bottomed flask charged with 50 mL of 0.1 M HCl solution. After stirring for 30 min, 2.70 g of $FeCl_3 \cdot 6H_2O$ (Mw=270.3 g/mol) in 10 mL of HCl solution was poured into the reaction system. The mixture was stirred for another 4 h and the precipitated product was collected by filtration. The crude product was washed by 0.1 M HCl for 6 times. To deprotonate the crude product, 500 mL of 2.0 M $NH_3 \cdot H_2O$ dissolved in 300 mL of acetone was mixed with the crude product and stirred for 30 min. At last, the acetone was removed through rotatory evaporation and the final product was obtained via filtration and desiccation. The yield of 4AT was 41%. ^{1}H NMR (400 MHz, DMSO-*d6*, ppm): 8.40 (*s*, 1H), 7.24 (*s*, 2H), 7.11 (*s*, 5H), 7.00-6.81 (*m*, 8H), 6.64 (*s*, 2H), 5.52 (*s*, 2H). ^{13}C NMR (100 MHz, DMSO-*d6*, ppm): 156.63, 154.58, 147.90, 142.90, 142.32, 141.34, 139.05, 136.15, 135.88, 134.56, 129.03, 124.33, 123.17, 119.81, 116.87, 113.89. MS (ESI) calculated for C24H20N4 [M]: 364.1688. Found: 365.1751 $[M+H]^+$.

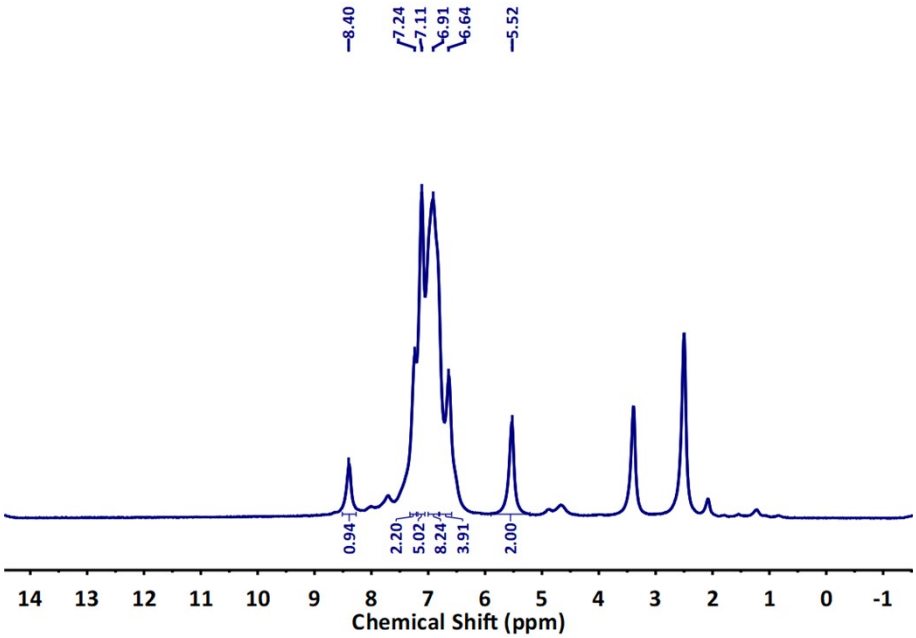

Figure S4. ^{1}H NMR spectrum of 4AT.

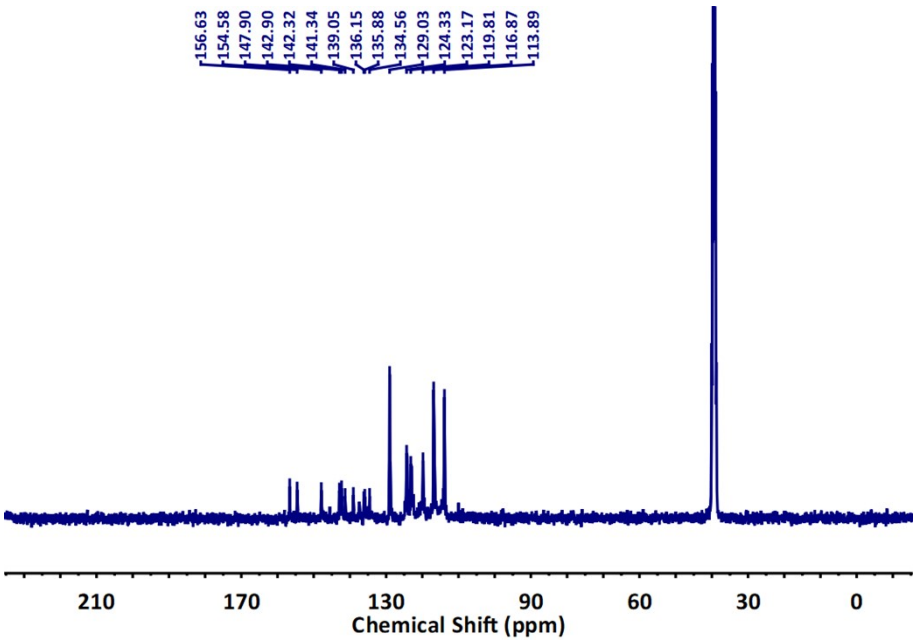

Figure S5. ^{13}C NMR spectrum of 4AT.

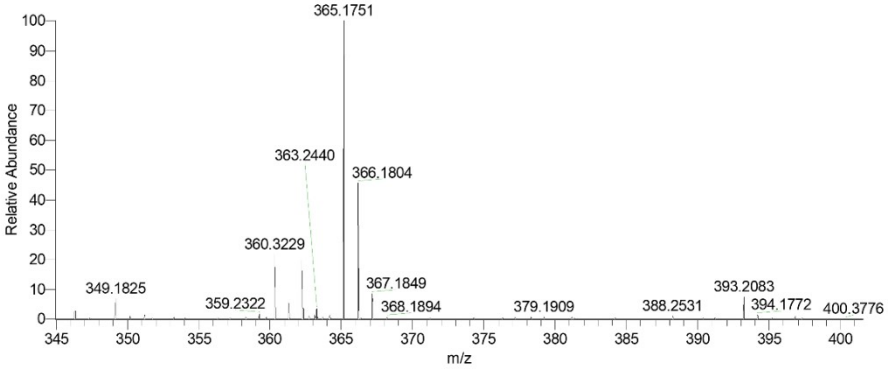

Figure S6. MS (ESI) spectrum of 4AT.

Phenyl capped aniline tetramer (5AT)

To a Schlenk tube, 483.6 mg of 4-aminodiphenylamine (Mw=184.24 g/mol) was added along with 43.1 mg of $Pd(dba)_2$ (Mw=915.72 g/mol), 70.1 mg of rac-BINAP (Mw=622.67 g/mol), 294.9 mg of 1,4-dibromobenzene (Mw=235.9 g/mol), and 360.4 mg of NaO(*t*-Bu) (Mw=96.10 g/mol). The mixture was dissolved by 40 mL of anhydrous toluene under the protection of nitrogen. The system was heated up to 110 ^{o}C and vigorously stirred for 24 h. After the mixture was cooled down to temperature, 675.9 mg of phenyl hydrazine (Mw=108.14) was added dropwise in order to prevent the oxidation of the crude product. The toluene was removed under reduced pressure, and the residue was washed with the mixed solvent of 100 mL of EtOH and 20 mL of water for 1 h. 5AT in a leucoemeraldine base form (5AT-LEB) could be obtained after removing the mixed

solvent via filtration. The yield of 5AT-LEB was 89%. ^{1}H NMR (400 MHz, DMSO-*d6*, ppm): 7.74 (*s*, 2H), 7.59 (*s*, 2H), 7.14-7.10 (*t*, 4H), 6.98-6.88 (*m*, 16H), 6.67-6.64 (*s*, 2H), 5.52 (s, 2H). ^{13}C NMR (100 MHz, DMSO-*d6*, ppm): 145.26, 138.74, 136.77, 134.44, 128.79, 120.48, 118.31, 117.58, 116.93, 114.28. MS (ESI) calculated for C30H26N4 [M]: 442.2157. Found: 442.2113 [M]. In addition to the synthesis of 5AT product, 221.3 mg of 5AT-LEB (442.6 mg) was dissolved in DMF. 114.1 mg of $(NH_4)S_2O_8$ in 20 mL of 2M HCl was added dropwise into the mixture. After stirring for 30 min, the reaction mixture was poured into 250 mL of water and stirred for another 15 min. The precipitation was collected via filtration and further added into a mixed solvent of 50 mL of 2.0M $NH_3{\cdot}H_2O$ and 200 mL of acetone. After stirring for 30 min, the acetone was removed under reduced pressure. The final product was collected through filtration and dried under vacuum under 45^{o}C. The yield of 5AT was 88%. MS (ESI) calculated for C30H24N4[M]: 440.2001. Found: 441.2072 $[M+H]^{+}$.

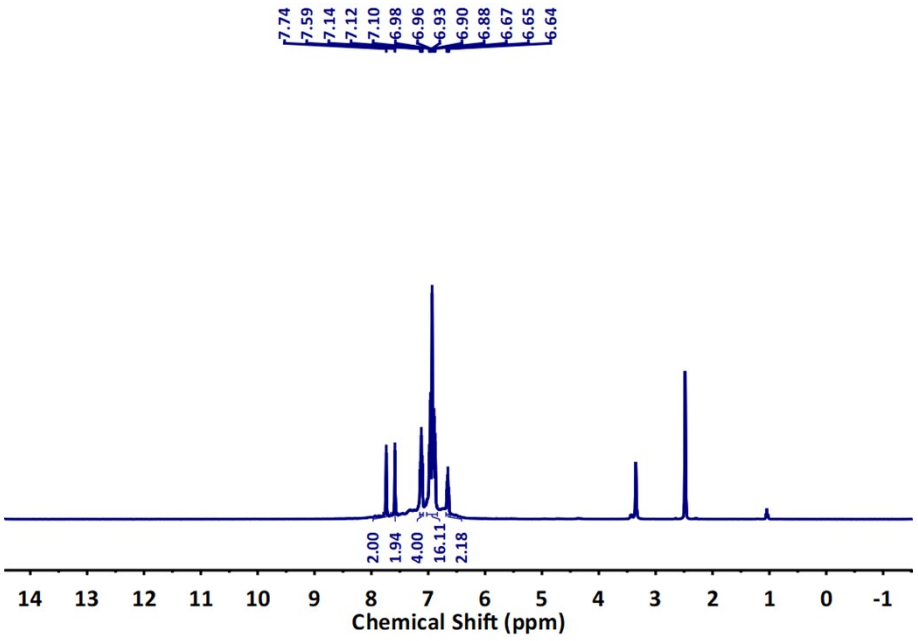

Figure S7. ^{1}H NMR spectrum of 5AT-LEB.

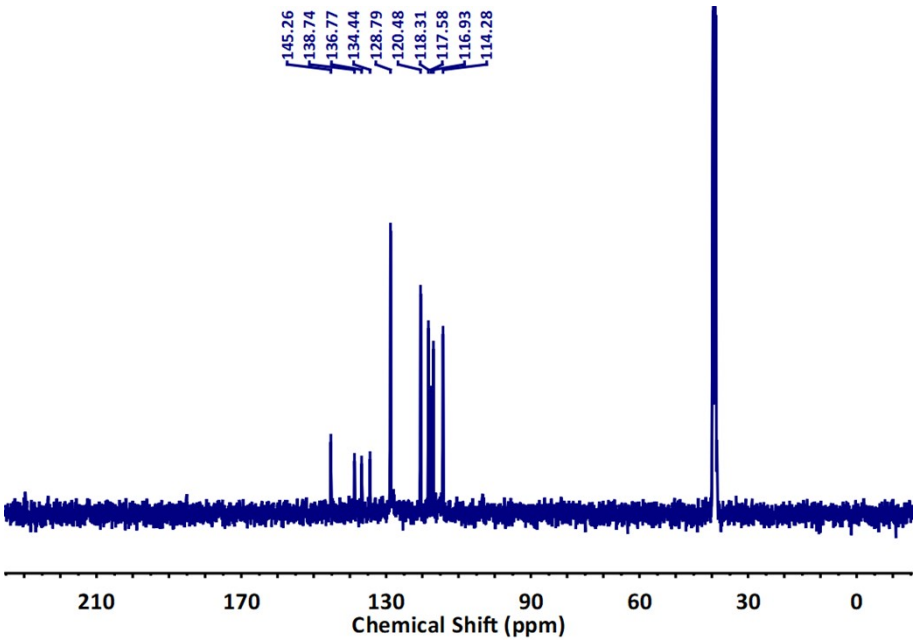

Figure S8. ^{13}C NMR spectrum of 5AT-LEB.

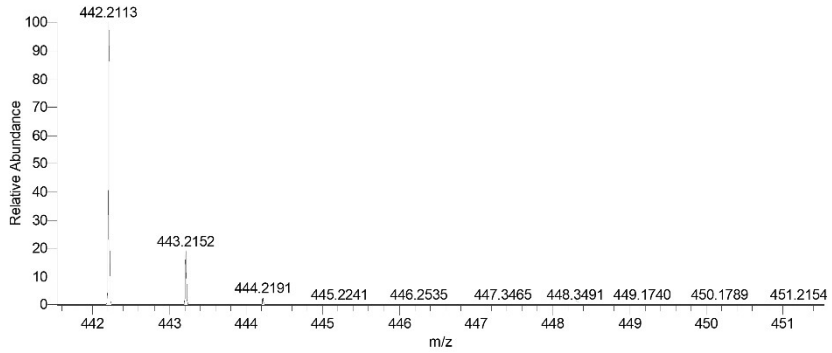

Figure S9. MS (ESI) spectrum of 5AT-LEB.

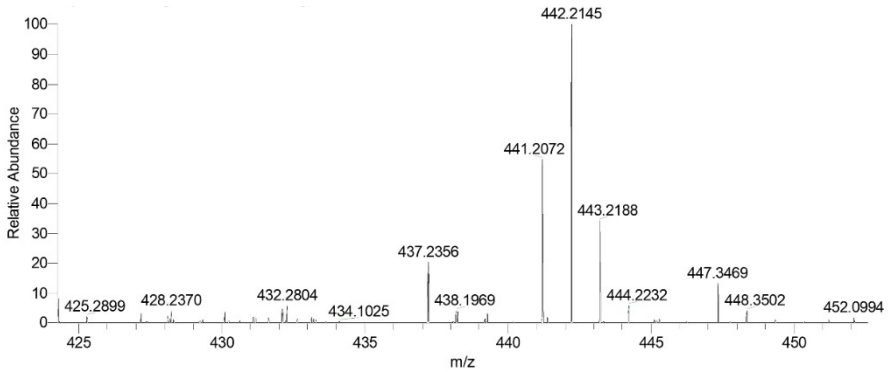

Figure S10. MS (ESI) spectrum of 5AT.

Measurement of mass extinction coefficient

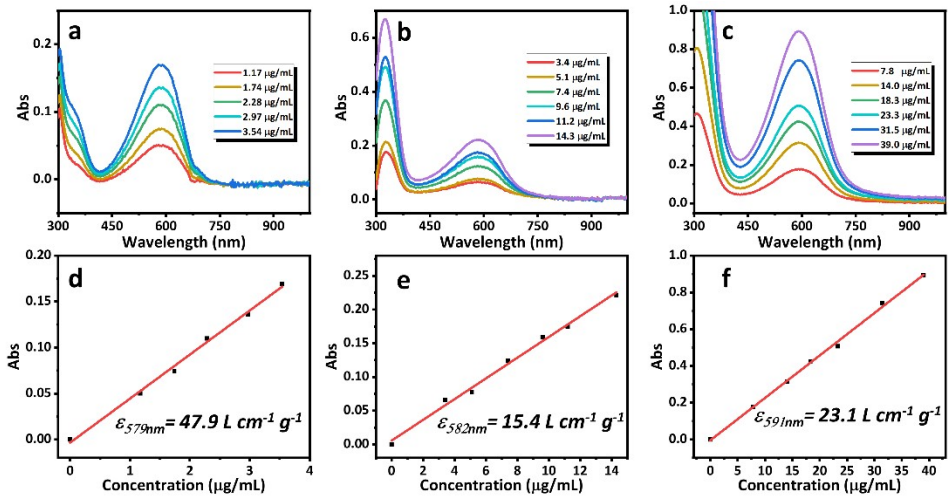

Figure S11. (a-c) Concentration-dependent UV-vis-NIR absorption spectra of 3AT (a), 4AT (b), and 5AT (c). (d) Fitting curve of the absorbance at 579 nm as a function of 3AT concentration. The $\varepsilon_{579\ nm}$ of 3AT is estimated as 47.9 L cm^{-1} g^{-1}. (e) Fitting curve of the absorbance at 582 nm as a function of 4AT concentration. The $\varepsilon_{582\ nm}$ of 4AT is estimated as 15.4 L cm^{-1} g^{-1}. (f) Fitting curve of the absorbance at 591 nm as a function of 5AT concentration. The $\varepsilon_{591\ nm}$ of 5AT is estimated as 23.1 L cm^{-1} g^{-1}.

Deprotonation of oligoanilines

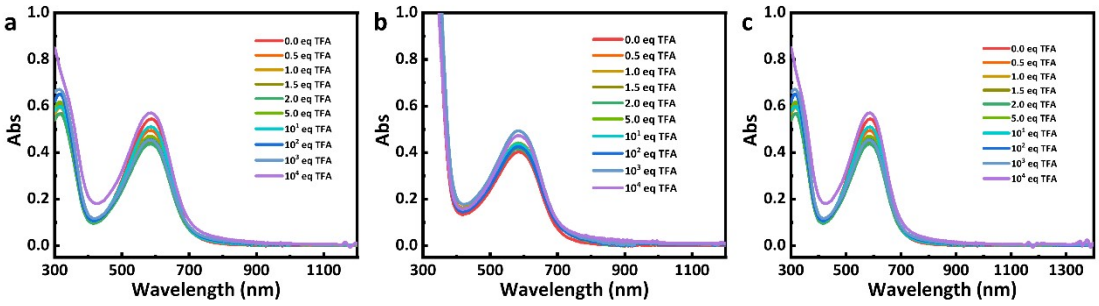

Figure S12. UV-vis-NIR absorption spectra of 3AT (a), 4AT (b), 5AT (c) deprotonated with TEA, after protonated by different concentrations of TFA.

Proposed doping mechanisms

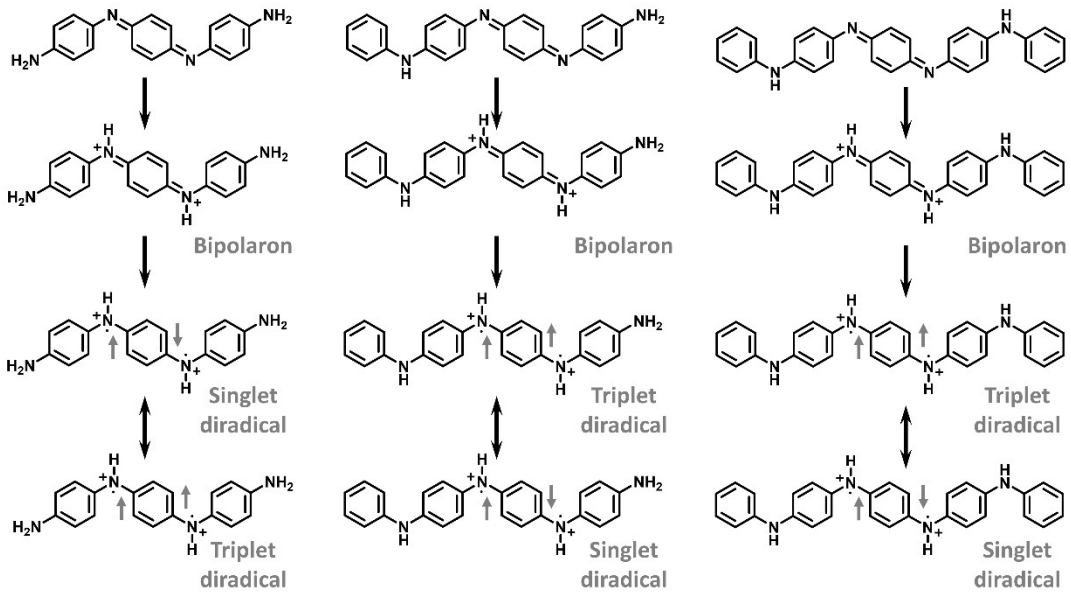

Figure S13. Proposed doping mechanisms of 3AT (left), 4AT (medial), and 5AT (right).

Superconducting quantum interference device (SQUID) measurement of 4AT

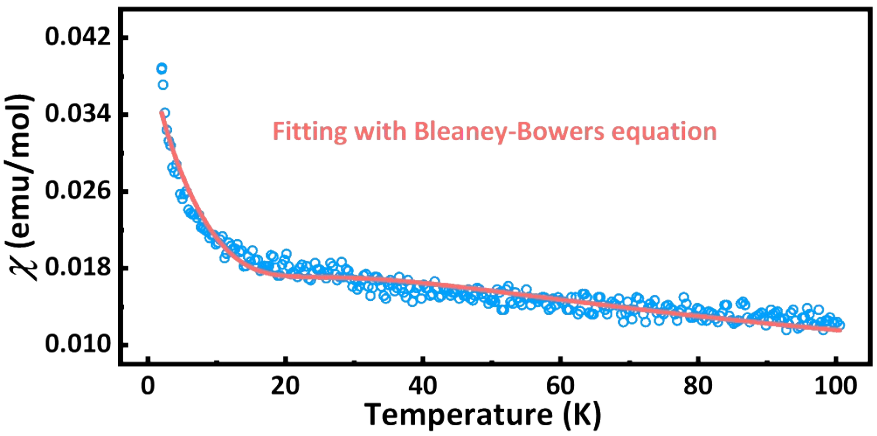

Figure S14. Superconducting quantum interference device measurement of 4AT doped by 10^3eq TFA in DMSO.

Density functional theory (DFT) calculations

Geometry optimizations and spectrum stimulations were performed in Gaussian 09. For geometry optimizations, the UB3LYP function was implemented and the standard 6-31g(d) basis set was employed. The outputs from geometry optimizations were applied as the starting points for time-dependent density functional theory (TD-DFT) calculations. The stimulated absorption spectra and the oscillator strengths of the absorption peaks were obtained by Multiwfn v3.8

software package. The molecular energy diagram, the spatial distribution of orbitals, and the hole-electron analysis were also carried out using Multiwfn v3.8 software package.

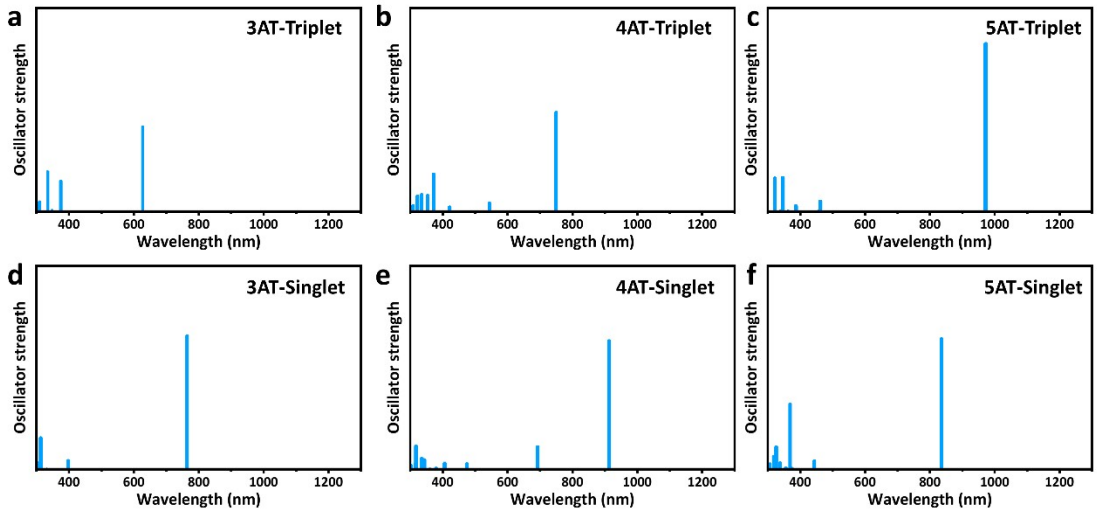

Figure S15. The oscillator strengths of the absorption peaks of triplet 3AT (a), 4AT (b), and 5AT (c) as well as singlet 3AT (d), 4AT (e), and 5AT (f).

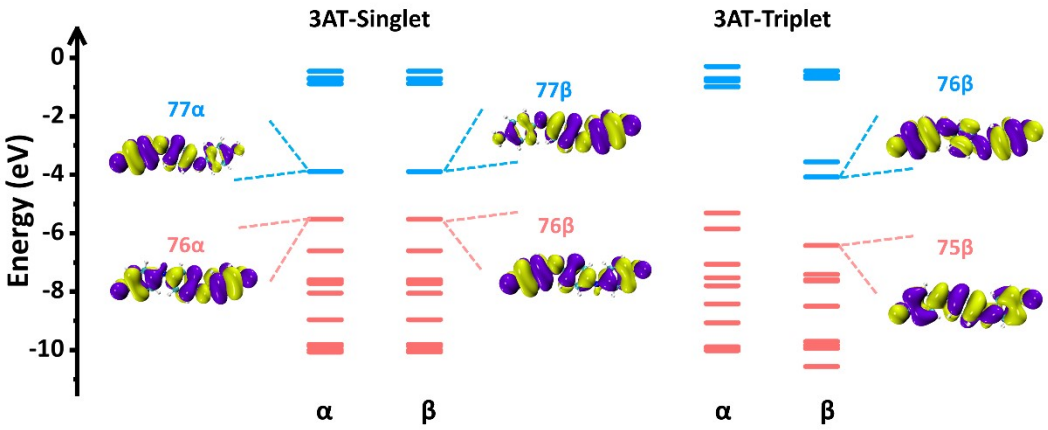

Figure S16. The molecular orbital energy diagram of 3AT at singlet sate and triplet state. The red and blue lines represent the occupied and unoccupied molecular orbitals, respectively. The spatial distribution of the lowest unoccupied molecular orbitals as well as highest occupied molecular orbitals are depicted (isovalue=0.002).

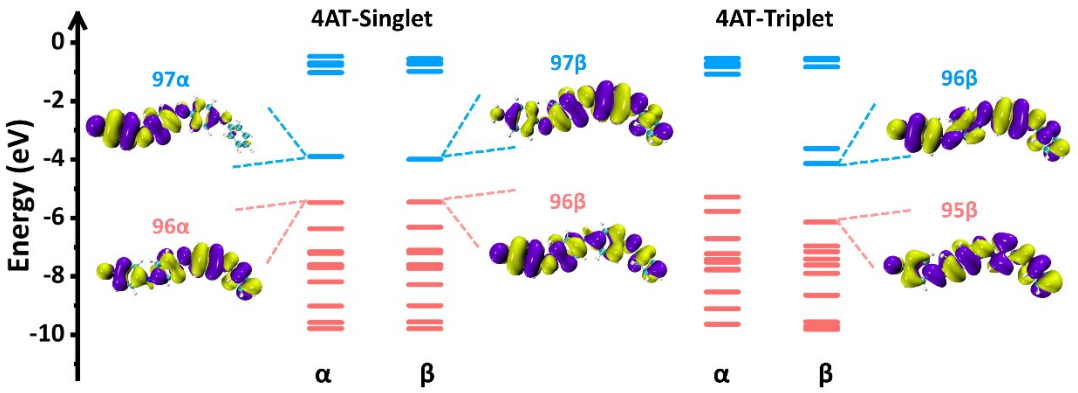

Figure S17. The molecular orbital energy diagram of 4AT at singlet sate and triplet state. The red and blue lines represent the occupied and unoccupied molecular orbitals, respectively. The spatial distribution of the lowest unoccupied molecular orbitals as well as highest occupied molecular orbitals are depicted (isovalue=0.002).

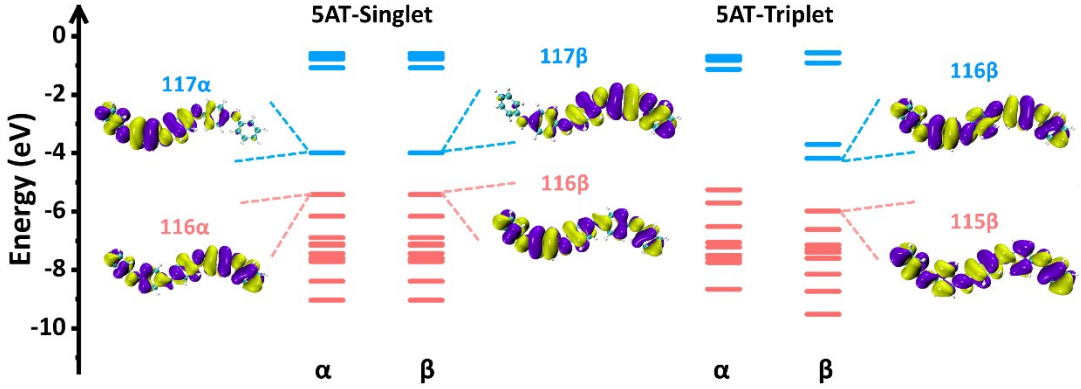

Figure S18. The molecular orbital energy diagram of 5AT at singlet sate and triplet state. The red and blue lines represent the occupied and unoccupied molecular orbitals, respectively. The spatial distribution of the lowest unoccupied molecular orbitals as well as highest occupied molecular orbitals are depicted (isovalue=0.002).

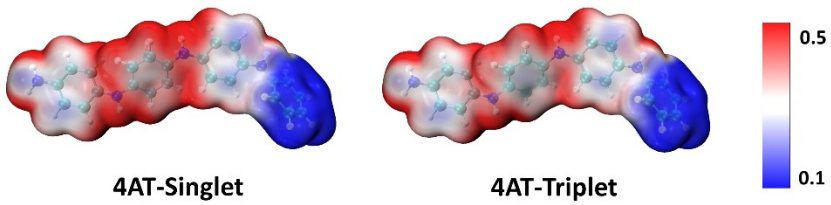

Figure S19. Calculated electrostatic potential surfaces of 4AT at singlet state and triplet state.

The measurements of NIR-I and NIR-II photothermal conversion and the calculation of photothermal conversion efficiency

All the photothermal conversion experiments were performed as following modality. To a quartz cell with optical distance of 0.1 cm, 0.1 mL of 100 μg/mL oligoaniline in DMSO-TFA solution was added. As such, the light absorbing area was fixed as 1.0 cm^2. NIR-I photothermal conversion was characterized upon the irradiation of 808 nm laser with the power density of 0.6 W/cm^2. NIR-II photothermal conversion was performed upon the irradiation of 1064 nm laser with the power density of 0.6 W/cm^2. The temperature changes were recorded by IR camera.

The photothermal conversion efficiency was calculated according to eq (1):

$$\eta = \frac{Q}{E} \tag{1}$$

Where Q refers to the generation of heat during photothermal conversion. E refers to the light power which is absorbed by the photothermal conversion system.

The thermal energy Q can be determined by summing the temperature increase in DMSO solution and thermal dissipation, as shown in eq (2):

$$mCp(T)\frac{dT}{dt} = Q - hA\Delta T \tag{2}$$

In which m and $C_p(T)$ represent to the mass and the specific heat capability of the photothermal conversion system which in this case mainly refers to DMSO. ΔT refers to the temperature change of the system. h and A are the thermal conductivity and heat dissipation area, respectively. The time-dependent temperature changes of the oligoanilines at different concentrations of TFA are well fitted with the eq (2). All the R-squared values are over 0.995, suggesting the eq (2) is suitable for evaluating heat generation.

The absorbed light power E can be specified by the eq (3) based on the basis of Lamber-Beer law:

$$E = P{\cdot}S{\cdot}(1 - 10^{-\varepsilon bc}) \tag{3}$$

where P refers to the power density of irradiation and S represents the absorbing area of the photothermal system (1 cm^2). ε is the mass extinction coefficient of oligoaniline in DMSO-TFA solution. c is the mass concentration of oligoaniline and b is the optical distance (0.1 cm).

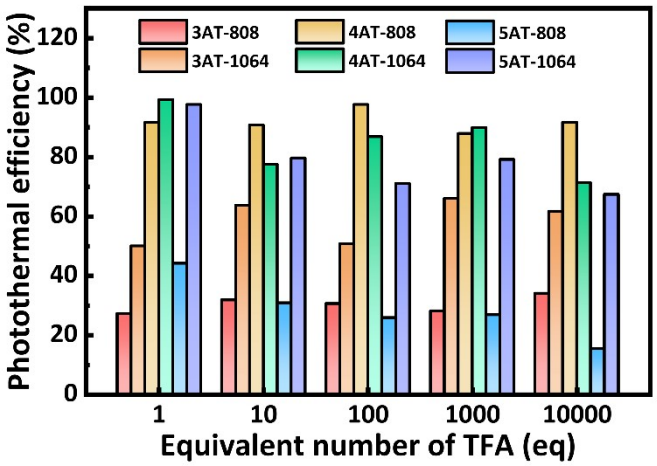

Figure S20. The calculated photothermal conversion efficiency of the oligoanilines in DMSO doped by different concentrations of TFA upon the irradiation of 808 nm and 1064 nm lasers, respectively.